THE JOURNAL OF BIOLOGICAL CHEMISTRY VOL. 281, NO. 15, pp. 10389–10398, April 14, 2006

Role of Heme Iron Coordination and Protein Structure in the Dynamics and Geminate Rebinding of Nitric Oxide to the H93G Myoglobin Mutant

*IMPLICATIONS FOR NITRIC OXIDE SENSORS**

Received for publication, December 15, 2005, and in revised form, February 8, 2006 Published, JBC Papers in Press, February 13, 2006, DOI 10.1074/jbc.M513375200

Michel Negrerie[‡§¶1], Sergei G. Kruglik[‡§¶‖], Jean-Christophe Lambry[‡§¶], Marten H. Vos[‡§¶], Jean-Louis Martin[‡§¶], and Stefan Franzen[**]

*From [‡]INSERM U696, Laboratoire d'Optique et Biosciences, Palaiseau F91120, France, [§]CNRS UMR 7645, Palaiseau F91120, France, [¶]Ecole Polytechnique, Palaiseau F91120, France, [‖]BioMoCeTi, CNRS UMR 7033, University Pierre & Marie Curie, Genopole Campus, 91030 Evry, France, and the **Department of Chemistry, North Carolina State University, Raleigh, North Carolina 27695*

The influence of the heme iron coordination on nitric oxide binding dynamics was investigated for the myoglobin mutant H93G (H93G-Mb) by picosecond absorption and resonance Raman time-resolved spectroscopies. In the H93G-Mb, the glycine replacing the proximal histidine does not interact with the heme iron so that exogenous substituents like imidazole may coordinate to the iron at the proximal position. Nitrosylation of H93G-Mb leads to either 6- or 5-coordinate species depending on the imidazole concentration. At high concentrations, (imidazole)-(NO)-6-coordinate heme is formed, and the photoinduced rebinding kinetics reveal two exponential picosecond phases (~10 and ~100 ps) similar to those of wild type myoglobin. At low concentrations, imidazole is displaced by the trans effect leading to a (NO)-5-coordinate heme, becoming 4-coordinate immediately after photolysis as revealed from the transient Raman spectrum. In this case, NO rebinding kinetics remain bi-exponential with no change in time constant of the fast component whose amplitude increases with respect to the 6-coordinate species. Bi-exponential NO geminate rebinding in 5-coordinate H93G-Mb is in contrast with the single-exponential process reported for nitrosylated soluble guanylate cyclase (Negrerie, M., Bouzhir, L., Martin, J. L., and Liebl, U. (2001) *J. Biol. Chem.* 276, 46815–46821). Thus, our data show that the iron coordination state or the heme iron out-of-plane motion are not at the origin of the bi-exponential kinetics, which depends upon the protein structure, and that the 4-coordinate state favors the fast phase of NO geminate rebinding. Consequently, the heme coordination state together with the energy barriers provided by the protein structure control the dynamics and affinity for NO-binding enzymes.

Nitric oxide acts as a signal transmitter in several physiological pathways (1–3) because it readily diffuses through cell membranes and reacts with the heme iron. It has been proposed that the ligation of NO[2] to myoglobin has a physiological role for the *in vivo* regulation of the NO concentration in muscle cells (4). Numerous hemoproteins are involved in diatomic ligand binding, such as CO, O_2, and NO, and their regulation closely depends upon the dynamic behavior of these ligands. We have shown that the dynamics of nitric oxide, and hence the geminate rebinding to the heme, are closely related to the protein function and subtly controlled by the protein structure. This control is evident when comparing endothelial NO synthase (5) and soluble guanylate cyclase (6), which are the source and the receptor of NO in cells, respectively, in which NO acts as a second messenger for signal transduction. These two proteins display a very contrasting behavior with respect to geminate rebinding of NO, which is multiphasic and relatively slow for endothelial nitric-oxide synthase, including important nanosecond phases correlated with the release of newly synthesized NO. On the other hand, NO recombination is mono-exponential and ultrafast for sGC, revealing a high trapping efficiency. The picosecond and nanosecond phases of the geminate recombination of a diatomic ligand to the heme (and its release from the heme) are modulated by several structural features linked to the intrinsic properties and function of hemoproteins. These features include the heme coordination state and protein structure whose respective contributions must be investigated for understanding the protein mechanism and regulation at the molecular level. Here we focus on the role of the iron proximal coordination in modulating the various phases of NO recombination.

NO is a particularly versatile and intriguing ligand because it can give rise either to 5-coordinate or to 6-coordinate adducts, the latter having the proximal histidine involved in the second axial coordination, and both conformations presenting biological importance. Although the NO adducts of wild type myoglobin or hemoglobin are observed to be 6-coordinate, binding of NO to sGC leads to an NO-5-coordinate Fe^{2+} complex after breaking the bond between the proximal His and the heme iron by a trans effect, which corresponds to a weakening of the axial Fe–*X* bond following the trans-coordination of a sixth ligand with ferrous iron (7, 8). The geminate recombination of NO to Mb or Hb always exhibits multiexponential kinetics on the picosecond time scale with two dominant phases (~10 and ~100 ps) for both proteins (9–13). The origin of this multiphasic behavior has led to several hypotheses that are not mutually exclusive. The first one attributes the dynamics to relaxation of the protein structure initiated by the iron motion after NO dissociation (10). The second hypothesis suggests that distal side chains present energy barriers to rebinding (14, 15), with a possible contribution of the position of the heme metal atom (16, 17). Contrary to Mb and Hb, a mono-exponential recombination of NO to the 4-coordinate Fe^{2+} after photodissociation is observed in sGC (6). On the other hand, the effects of distal mutations on the rebinding of NO to Mb (15, 17) or to

* This work was supported by National Science Foundation Grant MCB-9874895 (to S. F.) and grants from Fondation pour la Recherche Medicale, INSERM, and Ecole Polytechnique (to S. G. K.). The costs of publication of this article were defrayed in part by the payment of page charges. This article must therefore be hereby marked "*advertisement*" in accordance with 18 U.S.C. Section 1734 solely to indicate this fact.

[1] To whom correspondence should be addressed: Laboratoire d'Optique et Biosciences, INSERM U696, Ecole Polytechnique, 91128 Palaiseau Cedex, France. Tel.: 133-69-44-40; E-mail: michel.negrerie@polytechnique.fr.

[2] The abbreviations used are: NO, nitric oxide; WT Mb, wild type myoglobin; Im, imidazole; sGC, soluble guanylate cyclase; SVD, singular value decomposition; MEM, maximum entropy method; DFT, density functional theory. FeP, iron-porphyrin; DNP, double-ζ plus polarization; DNPP, double-ζ plus extra polarization.

leghemoglobin (18) suggest an important role for the amino acids in the distal pocket in governing the NO recombination rate. Thus, both the coordination state of the heme iron and the structure of the heme protein may influence the picosecond phases of NO geminate recombination and its bi-exponential character as suggested by the previous examples.

The H93G-Mb mutant provides a unique opportunity to investigate these effects in more detail. The H93G mutant lacks the proximal histidine that normally coordinates to the iron, and glycine does not interact with the heme so that exogenous substituents such as imidazole, phenol, or thiophene may coordinate to the heme iron (19). Imidazole mimics the proximal His coordination of WT Mb but is not covalently attached to the protein backbone. Moreover, the nitrosylation of H93G-Mb leads to either the 5- or the 6-coordinate form, depending on the concentration of exogenous imidazole. At imidazole concentrations less than 1 mM, the nitrosylated H93G-Mb is NO-5-coordinated, whereas above 1 mM it is 6-coordinated with spectroscopic properties similar to that of WT Mb (20–22). The H93G-Mb mutant is thus capable of mimicking both a 5-coordinate-NO complex like nitrosylated sGC and a 6-coordinate-NO form like Mb.

In this study, we have measured the fast rebinding kinetics of NO to H93G-Mb on the picosecond time scale by time-resolved absorption spectroscopy, and we identified the transient species by time-resolved resonance Raman spectroscopy. The results are compared with WT Mb and to sGC and provide insight into the structural factors that affect the geminate rebinding process. The experiments were followed by electronic potential energy surface calculations using DFT methods (23). The potential surfaces of 5- and 6-coordinate heme were calculated as a function of the distance between the free diatomic ligand NO and the heme iron.

EXPERIMENTAL PROCEDURES

To avoid confusion, the term "substituent" refers to the molecule bound at the proximal side of the heme in mutant Mb, replacing the coordinating histidine of WT Mb, although "ligand" refers to the diatomic molecule NO binding on the distal side.

Preparation of the Samples—The H93G-Mb mutant of sperm whale was overexpressed and purified as described (19). The expression was performed in the presence of imidazole. Removing of imidazole was achieved by ultrafiltration with successive concentration and dilution cycles in 5-kDa cut-off filters (Amicon). For exchange of the proximal substituents, the dilution was achieved with buffer (20 mM Tris, pH 7.4) containing the new substituent at final concentration that was 20 mM for imidazole, thiophene, and phenol, yielding the NO-6-coordinate heme, and it was 0.1 mM for the sample depleted in imidazole yielding an NO-5-coordinate heme. The samples were kept frozen (−80 °C) with a high concentration of imidazole, and the buffer exchange was performed immediately prior to the spectroscopic measurements.

The solution of ferric Mb mutant (100 μl at a concentration of 50 μM) was put in a 1-mm optical path length quartz cell (Hellma 110-QX) sealed with a rubber stopper and degassed by means of four successive cycles of vacuum and purging with pure argon. The heme iron was reduced by the addition of 10 μl of degassed sodium dithionite solution (5 mM final concentration). For preparing the NO-liganded species, gas phase NO diluted to 1% in N_2 (Alphagaz) was directly introduced into the spectroscopic cell by a syringe connected to the gas manifold, and a second silicone rubber stopper was stacked over the first one. The resulting NO concentration was 20 μM in the aqueous phase. Equilibrium spectra were recorded at each step for monitoring the evolution of ligation. Wild type myoglobin was similarly prepared from lyophilized powder (Sigma) dissolved in 50 mM Tris, pH 7.5. The absorbance of the sample was in the range 0.7–1 at the Soret maximum of liganded protein for 1 mm.

Soluble guanylate cyclase was purified from beef lung as described previously (6). Because it is directly purified in its ferrous state, no reducing agent was added. The final buffer was 25 mM triethanolamine, 50 mM NaCl, pH 7.5, and it was equilibrated with 1% NO gas phase in the same manner as Mb.

Picosecond Transient Absorption Spectroscopy—Transient spectra were recorded simultaneously to kinetics as a time-wavelength matrix data, using the pump-probe laser system described previously (24) and allowing the use of a white light continuum for generating the broad band probe pulse. The photodissociation of NO was achieved with an excitation wavelength in the a band at 560 nm with a pulse duration of about 40 fs and a repetition rate of 30 Hz. The transient absorption spectrum after a variable delay between pump and probe pulses was recorded by a CCD detector. The same 1-mm sample cell was used for recording the equilibrium spectra and the kinetics. The sample was continuously moved perpendicularly to the laser beam during the recording, and the temperature was 18 °C. The 100-ps time window was scanned with a dwell time of 1 s at each time point, and up to 40 scans were averaged. The two first spectra containing the cross-phase modulation artifact were removed. Analyses of the data were performed by a singular value decomposition of the time-wavelength matrix (25), and the kinetics associated with the SVD components having the highest singular value were fit to a minimum number of exponential components. The maximum entropy method analysis was performed on the kinetics obtained from SVD analysis.

Time-resolved Raman Spectroscopy—For sub-picosecond Raman spectroscopy, we used a femtosecond Ti:Sapphire oscillator pumped by a solid-state laser and producing 50-fs pulses ($\lambda = 810$ nm) subsequently amplified with a repetition rate of 1 kHz (26, 27). The output beam was frequency doubled at 405 nm and used to provide tunable pump and probe beams by means of an optical parametric generator and two optical parametric amplifiers based on BBO crystals. The photodissociating pulse energy was about 2 μJ in a sample cell with a 100-fs duration and had a wavelength centered at 560 nm. Narrow band interference filters allowed us to obtain probe pulses at a wavelength of either 420 nm (for 5C species) or 435 nm (for 6C species) and to achieve the best compromise between spectral (30 cm^{-1}) and temporal (0.6 ps) resolutions in time-resolved Raman measurements. The probe pulse energy was 20–30 nJ in the sample cell. The pump and probe beams were colinearly superimposed and focused on the sample, and the optical delay time between both pulses was controlled by a translation stage. Raman scattering light was collected through a spectrograph (Jobin-Yvon) by a CCD (Roper Scientific). The sample (100 μl) was placed in a cylindrical spinning cell whose gas phase contained the NO diluted in nitrogen. The integrity of the sample was verified after the experiment by recording its absorption spectrum in anaerobic conditions. Measurements were performed at 18 °C.

The spectrum before photodissociation at −5 ps (in the presence of the pump pulse) is that of the pure liganded species and was subtracted from that after NO dissociation (at +3 ps). It was multiplied by a coefficient (0.6 for these measurements) to suppress the contribution from still liganded species and to obtain a difference spectrum corresponding to the pure transient H93G Mb photoproduct.

Potential Energy Surfaces DFT Calculation—We have modeled potential energy surfaces by means of density functional calculations using the generalized gradient approximation (28) and the Becke-Lee-Yang-Parr functions (29) in the program DMol3 (30, 31). To calculate

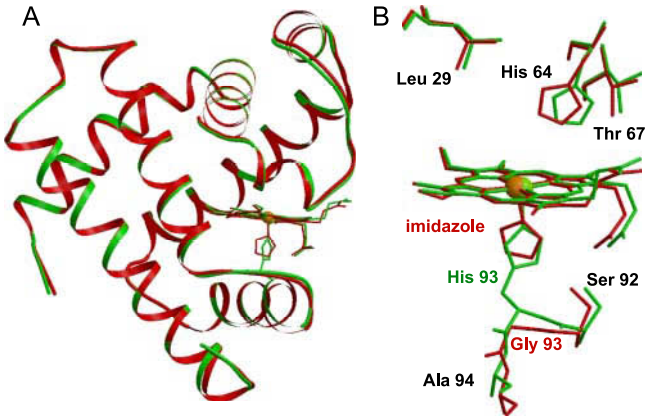

FIGURE 1. *A,* superposition of WT Mb structure (*green*) and that of the H93G mutant with imidazole as the proximal substituent (*red*). Both proteins are in the ferric state with a water molecule bound at the sixth iron coordination, so that the heme is planar. The structural data files obtained from the Protein Data Bank are 1BZ6 for sperm whale WT Mb (35) and 1IRC (19) for its H93G mutant. *B,* superposition of the heme, distal and proximal side chain. The superposition of structures was performed to maximize the number of common atomic positions, by means of the software Raster3D (33) and Molscript (34).

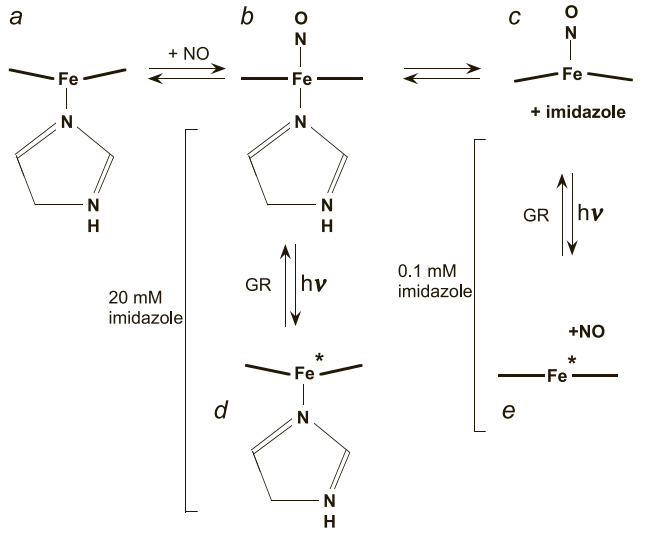

FIGURE 2. *a,* the five species of ferrous H93G Mb involved in this study are represented. The mutant H93G is purified in the presence of imidazole that remains bound at the proximal side of the heme both at 20 mM and 100 μM (*a*). However, because of the so-called "trans effect," the affinity for imidazole changes after NO binding to Fe^{2+}. At 2 mM imidazole, it remains bound as the proximal substituent and the heme iron is 6-coordinate (*b*) giving a transient 5-coordinate species (*d*) after NO release. When the imidazole concentration is lower, the ligation of NO results in a 5-coordinate iron (*c*) that leads to a transient 4-coordinate species after photodissociation of NO (*e*). *Fe** denotes an excited heme iron immediately after photodissociation ($t < 1$ ps), and GR stands for the geminate rebinding process.

the potential energy surface accurately, an extended basis set was used corresponding to a double-ζ plus two polarization functions (DNPP) as described elsewhere (23). All calculations were performed at the High Performance Computing resource at the North Carolina State University. The potential energy surfaces were generated for low spin $S = 1/2$, intermediate spin $S = 3/2$, and high spin $S = 5/2$ forms for Im-FeP-NO and FeP-NO (used in the geometry optimization). The potential energy surface of the total higher spin states of the system is assumed to be relevant for the dissociated form at the transition state, although the low spin forms correspond to the ground bound state (23, 32). The transition state is assumed to be in the geometry where the iron is in the heme plane of the (Im)-FeP-NO structures. The structures from the Protein Data Bank were compared by using the software Raster3D (33) and Molscript (34).

RESULTS

Steady-state Equilibrium and Imidazole Content—The mutation H93G induces neither a change of the protein fold (Fig. 1*A*) nor a change of the heme position (Fig. 1*B*) so that the overall structure is not perturbed. The superposition of WT (35) and mutant Mb (19) structures reveals only a slight rotation of the distal His-64. The absence of the proximal coupling between the heme and the backbone induces a relaxation of the helix end, leading to a slight change of the position of the peptide bonds 92–93 and 93–94. Compared with His-93, the exogenous imidazole, free from the constraint exerted by the helix F, appears rotated. The absorption spectra of unliganded WT and H93G-Mb(imidazole) are identical in both ferric and ferrous states. Fig. 2 depicts the five species depending upon the imidazole concentration, which are involved in the photodissociation experiments, and the steady-state spectra of the corresponding NO-liganded species are compared in Fig. 3*A*. When imidazole is the proximal substituent, the position of the maximum of the Soret band of NO-liganded mutant Mb depends upon concentration. In the presence of 20 mM imidazole (*i.e.* a concentration high enough for saturating the H93G-Mb at 50 μM), the absorption maximum is located at 418 nm when NO is bound (Fig. 3*A*). This wavelength is characteristic for an NO-6-coordinate species and is similar to that of WT Mb. Conversely, in the presence of 100 μM imidazole the binding of NO gives rise to a Soret maximum located at 399 nm, indicating that the equilibrium is displaced toward almost 100% NO-5-coordinate population. Indeed, this wavelength was observed for the endogenous NO receptor guanylate cyclase (6), which is a 5-coordinate nitrosylated species. The spectrum of the sample containing 100 μM imidazole exhibits an isosbestic point at 408 nm and a shoulder around 420 nm because of a very minor remaining population of 6-coordinate nitrosylated species. These observations are in agreement with the value of $K_D = 0.7$ mM for imidazole binding to the heme of the H93G-Mb at 295 K (22).

To investigate the influence of the nature of the proximal substituent itself, we replaced imidazole by phenol and thiophene in H93G-Mb. The absorption spectra of the corresponding NO-liganded H93G-Mb are compared in Fig. 3*B*. Included are the spectra of the CO-liganded mutant to compare the influence on both NO- and CO-6-coordinate species. Dialyzing the H93G-Mb with either thiophene or phenol even at concentrations as high as 20 mM always leads to a 5-coordinate species in the presence of NO (Soret band at 398 nm) because of a weaker bond strength between these proximal substituents and the heme iron; this indicates a much larger K_D value for these two substituents. The binding of CO to the imidazole-containing mutant only gives rise to the 6-coordinate species with a Soret band located at 421 nm. Similarly, CO does not displace thiophene or phenol but induces a slight shift to the Soret maximum at 418 nm, like for the 6C-NO species, indicating that whatever the substituent the proximally uncoupled 6-coordinate heme is slightly electronically perturbed, which is likely due to the relaxation of constraints within the heme pocket.

Geminate Rebinding of Nitric Oxide—Fig. 4 presents the transient absorption spectra associated with the geminate rebinding of NO after photodissociation from global analysis of the 100-ps data matrix. These SVD spectral components in Fig. 4 correspond to the highest singular value (27) and contain only a minor contribution from the excited electronic states relaxation that occurs in the 2–3-ps time-range (9, 36). This relaxation (not investigated here) presents a red-shift induced absorption (27) and has been separated as another SVD spectral component.

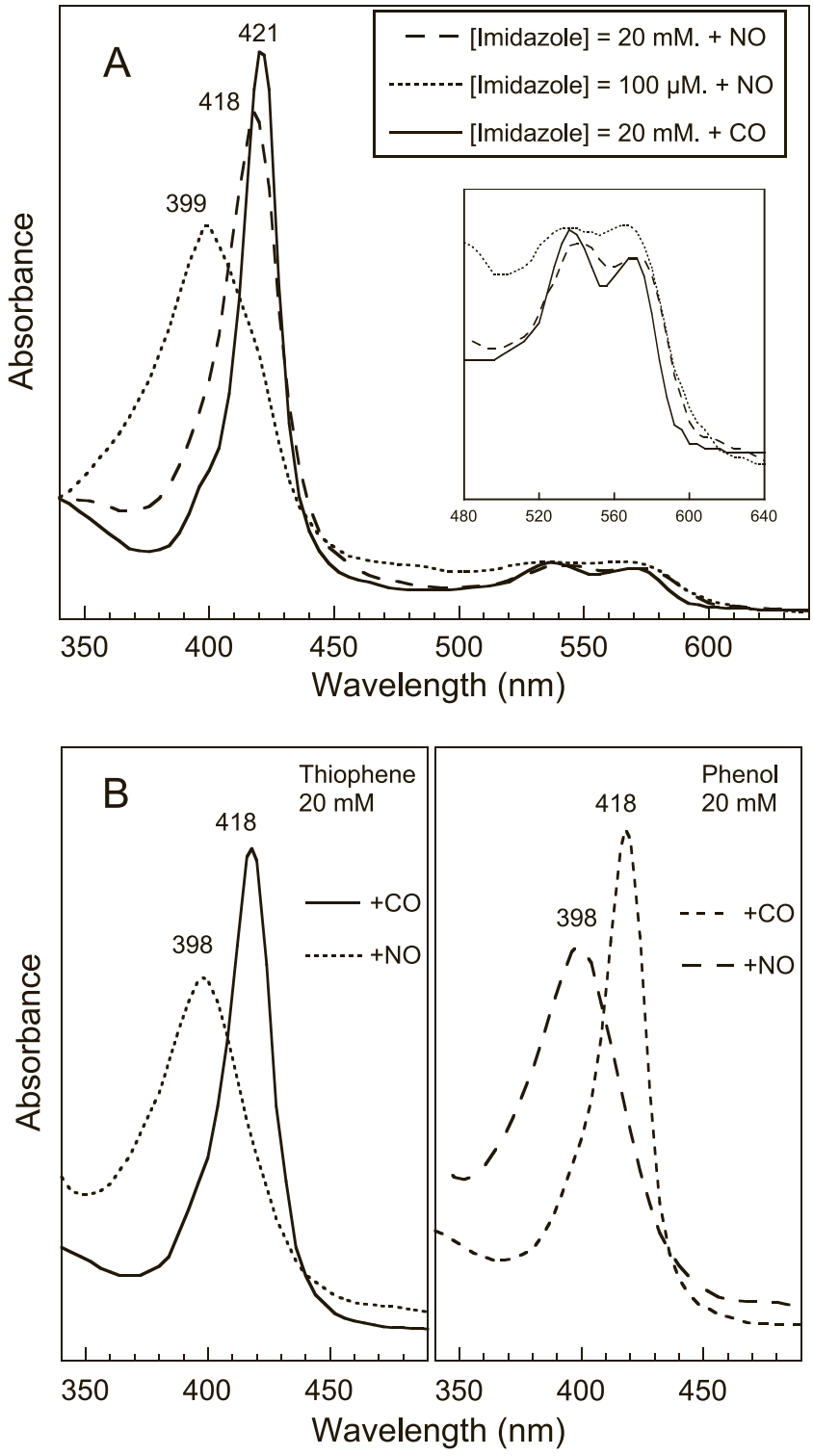

FIGURE 3. **Comparison of the absorption spectra of H93G mutant myoglobin reconstituted with three different proximal substituents and liganded with 1 mM CO and 2 μM NO.** *A*, different imidazole concentrations were used, 100 μM and 20 mM for the NO-liganded species and 20 mM for the CO-liganded mutant. *B*, spectra of mutants in buffer containing 20 mM thiophene and 20 mM phenol and incubated either with [NO] = 20 μM or [CO] = 1 mM.

The four substituted H93G-Mb mutants are compared with the WT Mb. More importantly, in the presence of 20 mM imidazole, the transient spectrum is very similar to that of WT Mb (Fig. 4*A*), with a bleaching maximum located at 418–420 nm and an induced absorption centered at 438 nm. This transient spectrum corresponds to the steady-state difference spectrum NO-liganded minus unliganded species and is thus characteristic of the photodissociation of an NO-6-coordinate ground state species with subsequent NO rebinding to a 5-coordinate photoproduct.

In contrast, for the lower imidazole concentration (100 μM), the difference spectrum possesses a minimum of bleaching at 400 nm shifted with respect to H93G-Mb at high imidazole concentration and a maximum of absorption at 434 nm. The bleaching at 400 nm corresponds to an NO-5-coordinate heme before photodissociation, and the NO rebinding should therefore occur to a 4-coordinate heme. Its transient spectrum is compared with that of guanylate cyclase (Fig. 4*B*) for which the photodissociation of NO induces a bleaching at 394 nm and creates a 4-coordinate transient species whose induced absorption discloses a

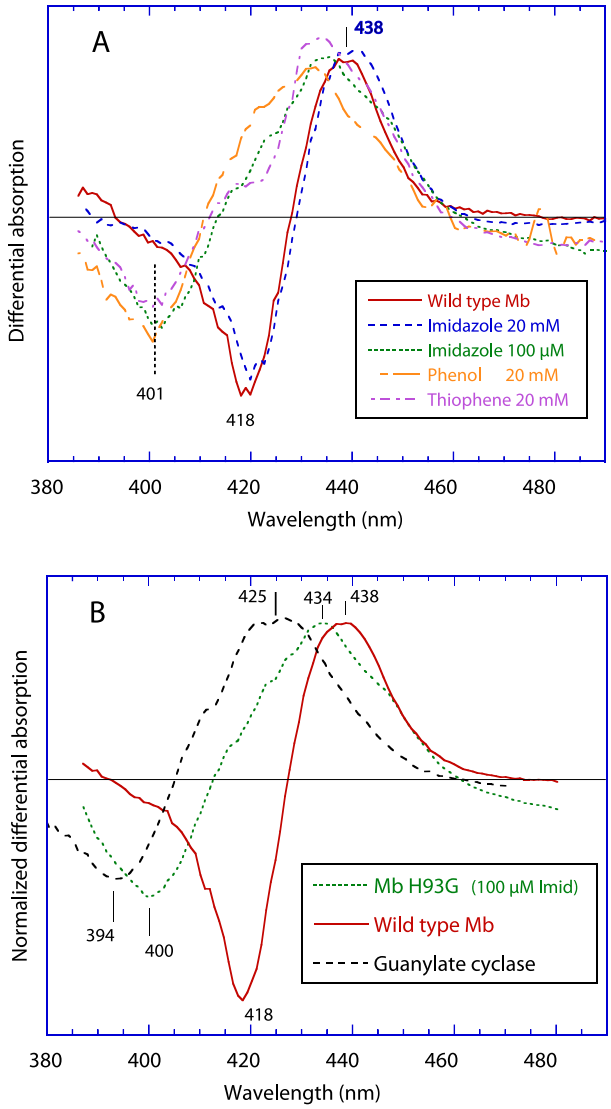

FIGURE 4. *A,* differential absorption transient spectra associated with the SVD kinetics component of NO rebinding process (*i. e.* without excited states contribution) to the five species. The H93G mutant is supplemented with 20 and 0.1 mM imidazole yielding a 6- and a 5-coordinate heme, respectively, and is compared with wild type myoglobin and with H93G mutant in the presence of 20 mM thiophene or 20 mM phenol. Only the differential spectra in the presence of 20 mM imidazole matches the equilibrium difference absorption spectra of unliganded Mb minus NO-liganded Mb. *B,* comparison of transient spectra from SVD analysis associated with the geminate rebinding for three proteins: WT myoglobin (*solid line*), H93G mutant myoglobin with 100 μM imidazole (*dashed line*), and soluble guanylate cyclase (*dotted line*).

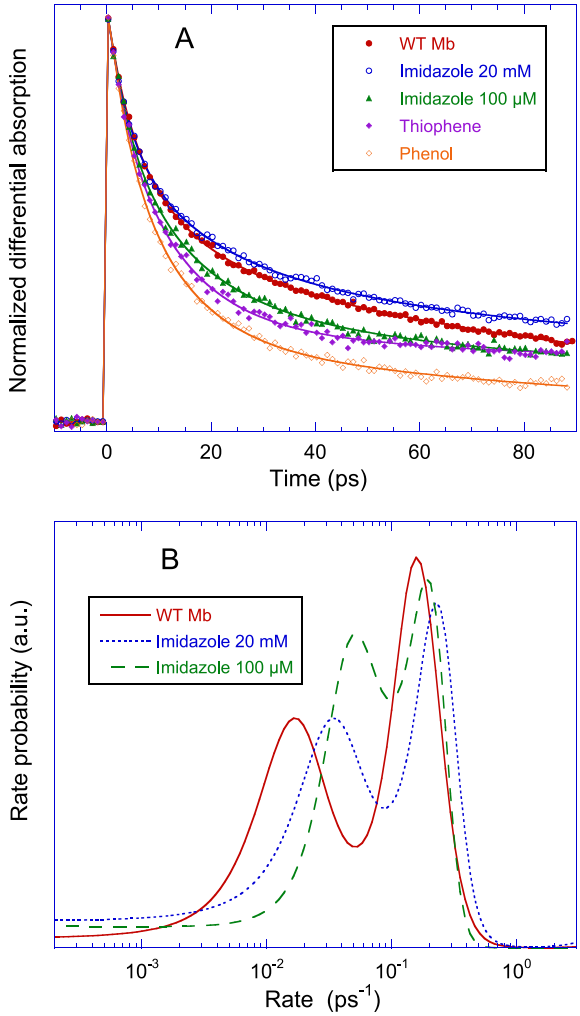

FIGURE 5. *A,* kinetic components associated with the transient differential spectra corresponding to NO rebinding (Fig. 4) for the wild type myoglobin and H93G mutants with the various proximal ligands. The traces are normalized, and the parameters of the fits (*solid lines*) are listed in Table 1. *B,* distribution of rates from the MEM analysis of NO rebinding kinetics of the wild type myoglobin compared with that of H93G imidazole-substituted mutants.

maximum centered at 425 nm. For both WT and H93G-Mb, no other SVD spectral component was observed, indicating the absence of intermediate species that would involve imidazole binding before or simultaneously to NO recombination. A small amount of 6C-NO mutant, as shown by a shoulder at 420 nm in the steady-state spectrum (Fig. 3*A*), leads to a shoulder located near 440–445 nm in the transient spectrum (Fig. 4*A*). We estimated this amount to be less than ~4%.

The transient difference spectra of the H93G-Mb samples containing 20 mM of either thiophene or phenol (Fig. 4*A*) are similar to that of H93G-Mb depleted of imidazole, consequently, the photodissociation of NO gives rise to a transient species similar to that obtained with 100 μM imidazole. This is consistent with a weaker bonding between iron and these two substituents than for imidazole liganded to H93G-Mb, as already suggested by the 3-nm down shift of the Soret band for CO-liganded mutant containing thiophene or phenol (Fig. 3*B*).

TABLE 1

Parameters from the bi-exponential fit of the 100-ps full kinetics

The data in Fig. 5 were fit using the function $A(t) = A_1 \exp(-t/\tau_1) + A_2 \exp(-t/\tau_2) + A_4 \exp(-t/3.5) + A_3$. The 3.5-ps component was added to the decay in order to take into account the photophysics of the heme. The relative amplitudes A_i do not include this fast component and thus describe only the NO rebinding process. The component τ_3 is assumed constant on the time scale used.

Protein	Equilibrium species	τ_1	A_1	τ_2	A_2	A_3
		ps		*ps*		
WT Mb	6C-NO	11	0.45	92	0.50	0.05
H93G Mb	(Im)-6C-NO	15	0.42	82	0.39	0.19
H93G Mb	Im[a] 5C-NO	15	0.63	95	0.25	0.12
H93G Mb	Thiophene[a] 5C-NO	12	0.73	116	0.14	0.13
H93G Mb	Phenol[a] 5C-NO	12	0.75	112	0.24	0.01
sGC[b]	5C-NO	7.5	0.97		0	0.03

[a] The exogenous ligand is displaced by NO in these cases.
[b] Data are from Ref. 6.

The kinetics of NO rebinding are compared in Fig. 5*A*. As displayed in Table 1, the data were fit to a three-exponential decay function and could not be correctly fit by a mono-exponential function. A 3-ps component takes into account the decay of the excited state (9), and two components correspond to the geminate recombination for all the proteins and substituents. These NO recombination components can be

labeled as a fast process (11–15 ps) and a slow process (82–116 ps) together with a constant whose amplitude varies but is always less than 19% of the total amplitude. The kinetics of NO recombination to WT Mb is consistent with that reported previously by Petrich *et al.* (15) having two exponential components. Our kinetic data clearly show that the contribution of the fast rebinding component increases for all the 5-coordinate-NO species regardless of the identity of the proximal substituent. For these species, it is assumed that the iron is 4-coordinate after photodissociation. There is clearly a change of the relative proportion of both picosecond components, as measured by the increase of the value of A_1 from 0.45 and 0.42 for WT Mb and imidazole-saturated H93G-Mb to the value of 0.63 for the 5-coordinate species substituted with imidazole up to 0.73–0.75 for the species substituted with thiophene and phenol. Only the 6-coordinate mutant (20 mM imidazole) shows a fast phase similar to that of the WT Mb (whose transient spectra are identical), with a somewhat larger amplitude of the constant term. The higher amplitude of the initial fast phase is measured for the phenol-substituted mutant with an almost vanishing constant component (Table 1).

The slightly lower value of A_1 obtained for the mutant with 0.1 mM imidazole compared with thiophene and phenol may be due to the presence of a small amount of 6-coordinate iron, the contribution of which is not resolved by the fit (*cf.* the shoulder in the spectrum Fig. 3*A* not present for thiophene and phenol). At 20 mM phenol and thiophene can still be present within the proximal pocket and induce slight differences in heme electronic environment, contrary to the case of 100 μM imidazole.

As an alternative to the fit to a bi-exponential function, we performed an analysis of the kinetics by MEM (37), which allows one to obtain the distribution of rates within the kinetics independently of a predefined kinetic model (Fig. 5*B*). The distributions have been normalized (in area) and represent the probability of the rate to have a particular value. More importantly, the MEM distribution of rates reveals two distinct peaks, corresponding to two rebinding phases within the kinetics for both coordination states. Furthermore, the probability of slower rebinding rates decreases for the NO-5-coordinate substituted mutant (100 μM imidazole) with respect to WT Mb. Thus, both independent methods of kinetic data analysis show the same trends.

Contrary to NO, in H93G-Mb the dynamics of photodissociated CO appears similar to that of WT Mb on a 300-ps time scale, where CO rebinding does not occur at all (data not shown), whatever the imidazole concentration. Thus, no perturbation of the heme pocket structure of H93G Mb occurs as seen in some distal mutants in which the energy barrier for CO escape is raised such that a picosecond phase appears (38).

Raman Spectra of Transient Species—To obtain an unambiguous signature of the transient species after NO dissociation, we measured the time-resolved Raman spectra of H93G-Mb in both coordination states, at −5 ps before and +3 ps after the photodissociation of NO. In the Fig. 6, *a* and *c*, are presented the ground-state Raman spectra of the 5C-NO species (H93G-Mb incubated in 100 μM imidazole) and its 6C-NO-Im counterpart (20 mM imidazole), both recorded at −5 ps. The heme modes ν_7 (674–678 cm^{-1}), ν_8 (345–348 cm^{-1}), and ν_9 (253–258 cm^{-1}) are clearly identified (39). Moreover, for the 5C-NO species in the ground state (Fig. 6, *spectrum a*) the stretching ν(Fe-NO) is seen at 534 cm^{-1} as a shoulder, as detected previously (40), which can be compared with the values obtained for other the 5C-NO proteins, 526 cm^{-1} for cytochrome *c*′ (41) and 520–525 cm^{-1} for sGC (42, 43). For both species, the transient spectrum was obtained by subtracting the ground state spectrum (−5 ps) from that after photodissociation (+3 ps). A

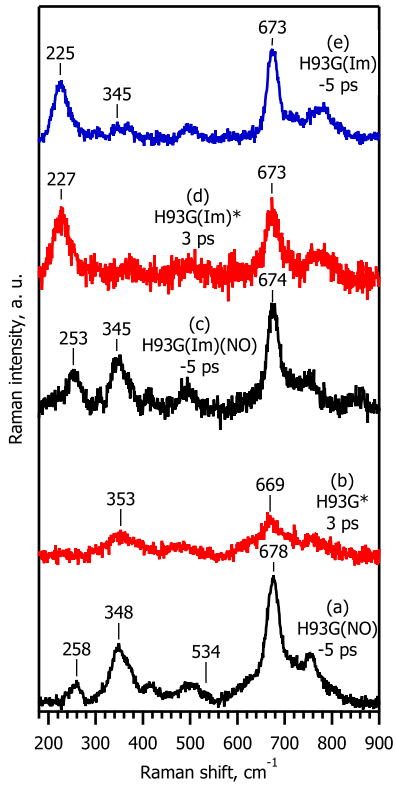

FIGURE 6. **Time-resolved resonance Raman spectra of ferrous H93G-Mb in various coordination states.** Spectra at −5 ps were recorded with the pump pulse arriving after the probe pulse and thus represent the ground-state scattering from the NO-5-coordinate (0.1 mM imidazole) (*a*), the Im-NO-6-coordinate (20 mM imidazole) (*c*), and the unliganded Im-5-coordinate (absence of NO) complexes (*e*). Difference spectra at 3 ps represent pure photoproduct scattering and originate from the 4-coordinate (*b*) and the Im-5-coordinate (*d*) transient H93G-Mb species. The assignment of vibrational modes is the following: ν_7 = 669–678 cm^{-1}; $\nu_{(Fe\text{-}NO)}$ = 534 cm^{-1}; ν_8 = 345–353 cm^{-1}; ν_9 = 253–258 cm^{-1}; $\nu_{(Fe\text{-}Im)}$ = 225–227 cm^{-1}.

coefficient (0.6) was iteratively determined and assigned to the (−5 ps) spectrum so that no negative signal appears in the difference spectrum (Fig. 6, *b* and *d*), which thus represents the pure photoproduct species at +3 ps.

Fig. 6, *a* and *b*, shows that for the 5C-NO mutant there is observable Raman intensity for the stretching ν(Fe-N$_{imid}$) (where ν(Fe-N$_{imid}$) is the stretching vibrational mode of the bond between iron and the nitrogen of imidazole) vibration neither in the equilibrium state (−5 ps) nor in the dissociated state (+3 ps), which appears at 225 cm^{-1} in the 5C ferrous H93G-Mb having imidazole as the axial ligand (Fig. 6*e*). Importantly, in the transient Raman spectrum of the photoproduct of 6C-(Im)-NO species (+3 ps, Fig. 6*d*), the ν (Fe-N$_{imid}$) stretching mode does clearly appear at 227 cm^{-1}, whereas this band is absent from the corresponding spectrum before photodissociation (−5 ps, Fig. 6*c*). The position of this band agrees well with that measured at 225 cm^{-1} in the −5 ps steady-state spectrum of ferrous 5C-(Im)-H93G-Mb without NO (Fig. 6*e*) and also with previously observed values for H93G-Mb after dissociation of CO (44) and for unliganded 5C-(Im)-H93G (45, 46). We note the absence of this mode in the case of the three 6C-CO-liganded proteins hemoglobin (44), WT Mb, and 6C-(Im)-H93G-Mb (46).

Potential Energy Surfaces—The DFT calculation allowed us to obtain simultaneously the structure of 5- and 6-coordinate FeP models and their related potential energy curves as a function of the Fe-NO distance. We briefly discuss here the validity of the calculated structures for different calculation methods with the aim of validating the potential energy curves.

The calculated potential energy surfaces of the FeP-(Im)-NO and FeP-NO model systems with respect to the Fe-NO distance are shown in Fig. 7. For both 5- and 6-coordination states of the model, the iron is in the plane defined by the four pyrrole nitrogens. Three calculations were carried out for comparative purposes, varying both the functional density and the basis set. The quality of the calculation is assessed by comparison of the calculated structures with known data from x-ray crystal structures (47, 48). The calculated and experimental structural parameters are listed in Table 2. The calculated Fe–NO and N–O bond lengths of the NO-(Im)-porphyrin model are 1.79 and 1.18 Å, respectively, using the generalized gradient approximation method with DNPP basis set. All the bond lengths and angles are in close agreement with the experimental x-ray structural data with a difference smaller than 0.08 Å in all cases, thus validating the calculations. The generalized gradient approximation method gave the best results, and the smaller basis set (DNP) gives slightly better agreement than the extended basis set.

The Fe–N–O bonds are bent for both 5- and 6-coordinate calculations and x-ray structures with an angle in the range 139–144° (Table 2), which is within 5° of the experimental angle in all cases (47). As expected, the angle Fe-N-O is higher for the calculated model than for Mb-NO (close to 111°; see Ref. 48) because there is no distal side chain exerting a steric constraint on the bound NO. Previous density functional calculations gave comparable results for 6-coordinate porphyrins (23), whereas Hartee-Fock calculations do not predict a bond between the iron and bound NO, but instead give values that are more consistent with a van der Waal's complex. The x-ray data of the 5C-NO-porphyrin at 295 K (47) revealed that the iron is displaced by 0.21 Å from the heme center toward NO, a value very close to those obtained by DFT calculations (Table 2). On the contrary the heme has a more planar configuration for 6C-NO porphyrin. Following NO dissociation, this geometry changes in both cases and can influence the rebinding.

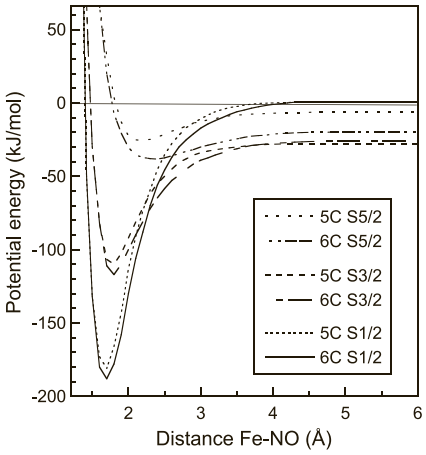

FIGURE 7. **Comparison of the potential energy surfaces with respect to the Fe-NO distance for the 5- and 6-coordinate NO species, both in the low spin (*LS, S* = 1/2), mixed spin (*MS, S* = 3/2), and high spin (*HS, S* = 5/2) states.** The corresponding calculated structural parameters are listed in Table 2.

The potential energy surfaces for both 5C and 6C species (in a planar geometry) compared in Fig. 7 are remarkably similar. The potential energy of binding for Fe-NO is −190 and −182 kJ/mol in the presence and absence of proximal imidazole, respectively, both for a system in a planar configuration and with a spin state $S = 1/2$. In all cases, the crossing points between the dissociated and the bound states curves do not give rise to an energy barrier to rebinding for either the 5C-NO or 6C-NO adducts. This should result in similar fast geminate recombination rates. These curves must also be compared with those performed in the nonplanar geometry case (23) as discussed below.

DISCUSSION

Interpretation of the Observed Transient Species—The H93G-Mb lacks the covalent bond between the protein backbone and the heme iron. This mutant has been expressed in the presence of imidazole to create a protein similar to the native myoglobin (19, 21) but differing in that there is no covalent bond between the imidazole and the protein. Different proximal substituents can be inserted into the heme pocket in place of imidazole by a simple dialysis, and none of them is covalently bound to the F-helix that contains Gly-93. Structural features influencing NO binding and dynamics emerge from the comparison of kinetics of the H93G Mb in the presence or absence of a proximal substituent due to the NO trans effect. Decatur *et al.* (22) have shown by absorption and steady-state Raman spectroscopy that in absence of substituent, H93G Mb is not 6- but 5-coordinate in its NO-liganded state. The characteristics of the NO-5-coordinate adduct include a Soret band centered 400 nm and a Raman spectrum with core-size marker bands shifted to values close to those of sGC spectrum. Indeed, as illustrated by the equilibrium spectra (Fig. 3), the trans effect exerted by NO promotes the dissociation of the axial ligand when the imidazole concentration is less than ~1 mM, whereas in the presence of 20 mM imidazole, the NO liganded H93G Mb is 6-coordinate.

The global analysis of the kinetics and transient spectra after photodissociation of the 6C-NO mutant revealed only two significant SVD components above the noise, corresponding to the excited state decay

TABLE 2

DFT calculation of structural parameters for the 5- and 6-coordinate model systems

Bond lengths (Å) and angle for Fe-N-O in 6- and 5-coordinate porphyrin models calculated using DFT methods are compared with that from experimental high resolution x-ray structural data of NO-bound porphyrin (Por) compounds (43). BLYP indicates Becke-Lee-Yang-Parr functions. Fe-Nϵ, Fe-Np, and *Qp* are the iron-histidine nitrogen bond lengths, iron-pyrrole nitrogen bond lengths, and out-of-plane iron displacement, respectively.

System	Method	Fe-NO	N-O	Fe-NO	Fe-Nϵ	Fe-Np	*Qp*
		Å	*Å*	*degrees*	*Å*	*Å*	*Å*
6-C NO							
Im-Por-NO	GGA (DNP)[a]	1.79	1.18	139	2.11	2.02	0.14
Im-Por-NO	GGA (DNPP)[a]	1.83	1.18	141	2.10	2.03	0.13
Im-Por-NO	BLYP (DNPP)[a]	1.74	1.19	140	2.28	2.03	0.21
1MeIm-(Fe)TTP-NO	Experiment[b]	1.75	1.17	139	2.17	2.01	0.07
5-C NO							
Por-NO	GGA (DNP)[a]	1.72	1.18	144		2.02	0.22
Por-NO	GGA (DNPP)[a]	1.78	1.18	139		2.02	0.20
Por-NO	BLYP (DNPP)[a]	1.82	1.19	139		2.04	0.22
(Fe)OEP-NO	Experiment[b]	1.72	1.17	144		2.00	0.29
(Fe)TTP-NO	Experiment[b]	1.72	1.12	149		2.01	0.21

[a] Calculation is from this work.
[b] Values are from x-ray structure of NO-bound porphyrin model compounds. See Ref. 47.

and to NO rebinding. If imidazole were photodissociated and not NO, then one would expect an induced absorption band centered around 399 nm due to a 5C-NO heme as in the sGC steady-state spectrum (6), which is not observed. There was no evidence for spectral components indicating a change in the proximal binding of imidazole, regardless of imidazole concentration. Therefore, we conclude that at 20 mM concentration the bound imidazole is not photodissociated, and that a concentration of 0.1 mM imidazole has a very low probability to rebind to Fe^{2+} in the proximal position before NO in the 100-ps time scale if still present within the proximal pocket.

The photodissociation of NO from the 5C-NO-H93G mutant induces a bleaching at 401 nm and an absorption increase centered at 434 nm, and we may assign this absorption increase to the 4-coordinate transient species based on the similarity with the transient spectrum of sGC. Furthermore, we have used transient Raman spectra to obtain a direct proof of the nature of the species. The comparison of time-resolved Raman spectra of 5C-NO and 6C-NO H93G-Mb before and after NO photodissociation directly identifies the transient species. In conditions yielding a 6C-NO-Im ground state mutant, the ν(Fe-N_{imid}) stretching mode (225 cm^{-1}) is absent before dissociation of NO (Fig. 6*c*). In fact, the ν(Fe-N_{imid}) mode is not sufficiently enhanced by resonance to be detected in 6C-heme (49, 50). In the transient Raman spectra of the photolyzed 6-coordinate species, the ν (Fe-N_{imid}) stretching mode is clearly present in transient spectra at +3 ps (Fig. 6*d*). This proves that the photolyzed intermediate (of the 6-coordinate NO adduct) is 5-coordinate and that the exogenous imidazole is not photodissociated and validates the above interpretation of the transient absorption spectra (Fig. 4).

On the other hand, the ν (Fe-N_{imid}) stretching mode is absent both before and after dissociation in the 5C-NO H93G-Mb spectra (Fig. 6, *a* and *b*). Furthermore, the porphyrin skeletal mode ν_9 at 253–258 cm^{-1} (51), which is strongly coupled to the iron-pyrrole breathing and C_β-C_1 bending modes (C_1 belongs to both propionate and vinyl chains), is prominent in the spectrum of the nitrosylated mutant species (Fig. 6, *a* and *c*), but it is weak or absent in the spectrum of unliganded or photodissociated species (Fig. 6, *b, c,* and *e*), as it was observed for the respective WT Mb forms (39, 52). This band appears at 253 cm^{-1} in the case of the NO-(Im)-H93G complex and disappears at +3 ps for both coordination states of the mutant, further proving that NO dissociation occurred. These data unambiguously show that the transient species is 4-coordinate after photoexcitation of the equilibrium 5C-NO heme of H93G-Mb throughout the time scale observed. We may thus assign the broad transient absorption band centered at 434 nm (Fig. 4) to the 4-coordinate heme.

Origin of the Bi-exponential Behavior for Nitric Oxide Geminate Rebinding—A remarkable result is that the amplitude of the fast picosecond rebinding component increases (0.42–0.63), whereas the time constant of the fast component does not change (τ_1 = 15 ps) when the iron is NO-5-coordinate NO-H93G Mb compared with the 6-coordinate species NO-(Im)-H93G Mb. The difference (11–15 ps) in the fast time constant observed between the WT and the H93G Mb (either 6C or 5C) is most probably associated with a slight relaxation of the protein structure caused by the covalent proximal decoupling in the mutant. Indeed, Barrick (19) observed differences, although slight, between x-ray structures of sperm whale WT and H93G Mb (see Fig. 1) corresponding to relieved strains within the heme surroundings. The role of the iron coordination must thus be inferred from the comparison between the 6C and 5C H93G-Mb species.

In H93G-Mb, the picosecond geminate rebinding to the 4-coordinate heme after photodissociation remains biexponential. In contrast, NO rebinding to the soluble guanylate cyclase (6), which also exhibits a 4-coordinate iron after photodissociation, is strictly mono-exponential and even more rapid (τ = 7.5 ps). Such a fast rate is consistent with a process occurring without any energy barrier. We can infer that the mono- or bi-exponential character of NO rebinding is determined by structural features in the distal heme pocket and protein structure. The iron coordination state and position are not sufficient in themselves to determine solely the rebinding kinetics.

Let us now compare the photoinduced kinetics obtained for 5C-NO-H93G with those for other systems possessing a 4-coordinated heme after photodissociation. The rebinding of NO to the heme alone in the ethylene glycol/water solution is mono-exponential, taking place in 7.5 ps (10, 53) without a slower picosecond component but with a constant base line (8%), which corresponds to the NO escape into the solvent, and whose amplitude depends upon the solvent composition (10). In fact, a bi-exponential recombination has never been observed for a heme in solution, *i.e.* without any protein environment. A similarly mono-exponential behavior has been measured for NO rebinding to microperoxidase (13), a heme-binding short peptide derived from cytochrome *c*. Thus, the protein structure itself induces the appearance of a second slow rebinding component (~100 ps), or even several slow components as in endothelial nitric-oxide synthase (5). The effect of the heme surroundings on the relative proportion of both picosecond phases is further observed by point mutations in the heme distal pocket. Mutants like V68A human Mb (15) and V68F sperm whale Mb (17) disclose an almost complete or complete bi-exponential picosecond rebinding. On the contrary, other mutants like V68I (17) or a triple mutation within the distal pocket (54) show a base-line amplitude because of the escape of NO from the pocket much larger than the WT Mb, but the NO rebinding remains bi-exponential whatever the mutation. In the soybean leghemoglobin, distal mutations of His-61 induce a dramatic increase of the fast phase amplitude, from 23 to 90% with no constant term, for the wild type and H61L mutant, respectively (18). Together, these and our results emphasize the role of the heme protein structure and heme pocket in the origin of the energy barriers controlling the component partitioning of the bi-exponential geminate recombination. These barriers may be static as well as depending upon protein relaxation (9, 13).

When NO rebinds to Mb in high viscosity media such as glycerol, the partitioning between the two rebinding phases changed but not the time constant of the fast phase (55). Although the rate of the rapid phase is independent of solvent viscosity, the relative amplitude and the rate constant of the slower phase both decrease on larger viscosity, with a simultaneous increase of the NO population recombining directly with a fast rate. This was interpreted (55) as a dependence of protein structural relaxation upon the viscosity and supports different origins of the barriers for the two picosecond recombination phases.

Potential Energy Surface Calculations and Geminate Rebinding—We have performed density function calculations to compare the potential energy surfaces of the molecular systems MeIm-FeP-NO and FeP-NO modeling H93G(Im)-NO and H93G-NO mutants Mb, respectively, and possessing a planar heme. We compared their energy barriers with the kinetic data. These potential energy surfaces apply to the heme-NO interaction without taking into account the protein surroundings of the heme, and thus they correlate with the fastest geminate rate. One might have anticipated a large difference between the barriers to recombination in the 5- and 6-coordinate species, which could have led to a difference in the geminate rate itself. However, the calculated potential energy surfaces reveal that for both 5-coordinate and 6-coordinate NO species there is no barrier for the S = 3/2 to S = 1/2 spin state change

and no crossing for $S = 5/2$ to $S = 3/2$ because of the position of curves crossing (Fig. 7). Both 5- and 6-NO-coordinate species have surprisingly similar potential energy surfaces in the ground states, corresponding to the similar rebinding rates observed in Fig. 5. The absence of a barrier from DFT calculation corroborates the data obtained by ultrafast transient absorption spectroscopy showing that the fast geminate recombination rate constants are similar in both H93G(Im)-NO and H93G-NO (*i.e.* 5- and 4-coordinate systems after NO photodissociation). These results agree with the involvement of structural factors such as architecture of the distal pocket in controlling the relative amplitude of both picosecond geminate phases.

It is noteworthy that a recent study led to a similar conclusion by means of a different approach than in our present work. Ionascu *et al.* (56) showed that the slow 100-ps component is temperature-dependent whereas the fast one (10 ps) is not, demonstrating that both kinetic components constitute separate processes. The fast process is thus shown to occur without enthalpic barrier. Furthermore, the rate of the fast phase was observed independent of the distal mutation V68W, which in contrast almost abolished the amplitude of the slow phase (100 ps). Their results (56) are consistent with an assignment of the slow phase to the rebinding of NO localized in a more distant site than the distal heme pocket, and thus experiencing a barrier to rebinding because of the protein structure (to which the Val-68 side chain participates).

Beside the coordination state, the position of the iron may play a role, as pointed out by previous comparative DFT calculations (23). Although these calculations indicated no energy barrier for a heme plane-iron distance $Qp \leq 0.2$ Å (where Qp is the distance between the iron and its projection of the plane defined by the nitrogen pyrroles), a barrier to rebinding appeared for $Qp = 0.4$ Å and correlates with more negative potential energies. According to these calculations (23), it thus appears that for an Fe-NO distance just above the Landau-Zener transition crossing (about 3 Å) the in-plane position of the iron facilitates NO rebinding compared with an out-of plane position because of the absence of barrier. This may explain the larger amplitude of the 10-ps phase of rebinding that we observed for NO-H93G-Mb. Whether NO does not move beyond this transition distance and is kept in proximity to the heme iron must depend on energy barrier(s) to escape from the distal pocket inherent to the protein structure, resulting in a decrease of k_{off}.

Implications for the Mechanism of NO Receptors—Heme proteins that function as receptors for NO have an overall structure that exerts a strain upon the proximal histidine. This strain induces a weakening of the His–Fe bond, which leads to the cleavage of the Fe–Nϵ bond upon binding of NO at the distal position (trans effect). Examples include guanylate cyclase, the mammalian endogenous receptor of NO, as well as the bacterial cytochrome *c′* from *Alcaligenes xylosoxidans* (41, 57), which possesses a structure different from that of sGC. If the protein structure reaches an energy minimum to accommodate the free proximal His side chain position, as suggested by calculations (58), the 5-coordinate-NO form is stable. In such species, the probability of fast NO rebinding after dissociation (thermal or photoinduced) is increased and becomes closer to single exponential as observed in sGC and corroborated by the NO rebinding kinetics in 5-coordinate NO-H93G Mb. The comparison of NO dynamics between Mb, its H93G mutant, and sGC suggests that the NO rebinding behavior is an intrinsic property of the protein structure and more specially of the distal pocket providing energy barriers. Furthermore, the heme in-plane position of the iron immediately after NO dissociation plays a role in increasing the probability of immediate rebinding, and advantage is taken of this effect by breaking the bond to the proximal histidine, a consequence of the structural adaptation of heme receptors to their function.

In conclusion, the bi-exponential character of the nitric oxide recombination kinetics to the heme is not because of the iron coordination state or to the motion of the proximal histidine, but rather it results from the presence of two spin channels for recombination that are modulated by protein structure and dynamics in the distal pocket. The fast process is only weakly affected by the structure of the distal pocket, although the slow process depends more strongly on energy barriers. The comparison of recombination to both 5- and 6-coordinate hemes in a similar distal environment in H93G-Mb provides information for the understanding of other heme proteins such as NO receptors. The overall effect of change of the trans ligation state in the NO rebinding kinetics of NO-H93G-Mb is surprisingly small, suggesting that indeed subtle distal structural factors give rise to a mono-exponential rebinding in guanylate cyclase and related proteins. We conclude that the mono-exponential rebinding of NO to sGC is not because of the 4-coordinated heme but is induced by the heme pocket and protein structure that decreases the probability of localization of the ligand far from the iron. The calculations show that the in-plane position of the iron favors the rebinding of NO when it is located within the heme pocket, as measured by the increase of the amplitude of the faster component. This effect together with the energy barriers on the ligand pathway provided by the protein structure result in two synergistic means for controlling the ligand binding, dynamics and affinity, and consequently may provide a regulation of the physiological activity of heme enzymes for which NO is an effector.

REFERENCES

1. Denninger, J. W., and Marletta, M. A. (1999) *Biochim. Biophys. Acta* **1411,** 334–350
2. Cooper, C. E. (1999) *Biochim. Biophys. Acta* **1411,** 290–309
3. Rodgers, K. R. (1999) *Curr. Opin. Chem. Biol.* **3,** 158–167
4. Flögel, U., Merx, M. W., Gödecke, A., Decking, U. K., and Schrader, J. (2001) *Proc. Natl. Acad. Sci. U. S. A.* **98,** 735–740
5. Negrerie, M., Berka, V., Vos, M. H., Liebl, U., Lambry, J. C., Tsai, A. L., and Martin, J. L. (1999) *J. Biol. Chem.* **274,** 24694–24702
6. Negrerie, M., Bouzhir, L., Martin, J. L., and Liebl, U. (2001) *J. Biol. Chem.* **276,** 46815–46821
7. Ignarro, L. J., Ballot, B., and Wood, K. S. (1984) *J. Biol. Chem.* **259,** 6201–6207
8. Zhao, Y., Brandish, P. E., Ballou, D. P., and Marletta, M. A. (1999) *Proc. Natl. Acad. Sci. U. S. A.* **96,** 14753–14758
9. Petrich, J. W., Poyart, C., and Martin, J. L. (1988) *Biochemistry* **27,** 4049–4060
10. Petrich, J. W., Lambry, J. C., Kuczera, K., Karplus, M., Poyart, C., and Martin, J. L. (1991) *Biochemistry* **30,** 3975–3987
11. Olson, J. S., and Phillips, G. N. (1996) *J. Biol. Chem.* **271,** 17593–17596
12. Ye, X., Demidov, A., and Champion, P. M. (2002) *J. Am. Chem. Soc.* **124,** 5914–5924
13. Kim, S., Jin, G., and Lim, M. (2004) *J. Phys. Chem. B* **108,** 20366–20375
14. Gibson, Q. H., Regan, R., Elber, R., Olson, J. S., and Carver, T. E. (1992) *J. Biol. Chem.* **267,** 22022–22034
15. Petrich, J. W., Lambry, J. C., Balasubramanian, S., Lambright, D. G., Boxer, S. G., and Martin, J. L. (1994) *J. Mol. Biol.* **238,** 437–444
16. Ikeda-Saito, M., Dou, Y., Yonetani, T., Olson, J. S., Li, T., Regan, R., and Gibson, Q. H. (1993) *J. Biol. Chem.* **268,** 6855–6857
17. Kholodenko, Y., Gooding, E. A., Dou, Y., Ikeda-Saito, M., and Hochstrasser, R. M. (1999) *Biochemistry* **38,** 5918–5924
18. Chowdhury, P. K., Kundu, S., Halder, M., Das, K., Hargrove, M. S., and Petrich, J. W. (2003) *J. Phys. Chem. B* **107,** 9122–9127
19. Barrick, D. (1994) *Biochemistry* **33,** 6546–6554
20. Decatur, S. M., De Pillis, G. D., and Boxer, S. G. (1996) *Biochemistry* **35,** 3925–3932
21. DePillis, G. D., Decatur, S. M., Barrick, D., and Boxer, S. G. (1994) *J. Am. Chem. Soc.* **116,** 6981–6982
22. Decatur, S. M., Franzen, S., De Pillis, G. D., Dyer, R. B., Woodruff, W. H., and Boxer, S. G. (1996) *Biochemistry* **35,** 4939–4944
23. Franzen, S. (2002) *Proc. Natl. Acad. Sci. U. S. A.* **99,** 16754–16759
24. Martin, J. L., and Vos, M. H. (1992) *Annu. Rev. Biophys. Biomol. Struct.* **21,** 199–222
25. Press, W. H., Teukolsky, S. A., Vetterling, W. T., and Flannery, B. P. (1988) *Numerical Recipes*, pp. 59–70, Cambridge University Press, New York
26. Cianetti, S., Negrerie, M., Vos, M. H., Martin, J. L., and Kruglik, S. G. (2004) *J. Am. Chem. Soc.* **126,** 13932–13933
27. Negrerie, M., Cianetti, S., Vos, M. H., Martin, J. L., and Kruglik, S. G. (2006) *J. Phys.*

Chem. B., in press
28. Perdew, J. P., Chevary, J. A., Vosko, S. H., Jackson, K. A., Pederson, M. R., Singh, D. J., and Fiolhais, C. (1992) *Phys. Rev. B* **46,** 6671–6687
29. Becke, A. D. (1997) *J. Chem. Phys.* **107,** 8554–8560
30. Delley, B. (1990) *J. Chem. Phys.* **92,** 508–517
31. Delley, B. (2000) *J. Chem. Phys.* **113,** 7756–7764
32. Franzen, S. (2002) *J. Phys. Chem.* **106,** 4533–4542
33. Merritt, E. A., and Bacon, D. J. (1997) *Methods Enzymol.* **277,** 505–524
34. Kraulis, P. J. (1991) *J. Appl. Crystalllogr.* **24,** 946–950
35. Kachalova, G. S., Popov, A. N., and Bartunik, H. D. (1999) *Science* **284,** 473–476
36. Franzen, S., Kiger, L., Poyart, C., and Martin, J. L. (2001) *Biophys. J.* **80,** 2372–2385
37. Steinbach, P. J., Chu, K., Frauenfelder, H., Johnson, J. B., Lamb, D. C., Nienhaus, G. U., Sauke, T. B., and Young, R. D. (1992) *Biophys. J.* **61,** 235–245
38. Sugimoto, T., Unno, M., Shiro, Y., Dou, Y., and Ikeda-Saito, M. (1998) *Biophys. J.* **75,** 2188–2194
39. Hu, S., Smith, K. M., and Spiro, T. G. (1996) *J. Am. Chem. Soc.* **118,** 12638–12646
40. Thomas, M. R., Brown, D., Franzen, S., and Boxer, S. G. (2001) *Biochemistry* **40,** 15047–15056
41. Andrew, C. R., Kemper, L. J., Busche, T. L., Tiwari, A. M., Kecskes, M. C., Stafford, J. M., Croft, L. C., Lu, S., Moenne-Loccoz, P., Huston, W., Moir, J. W. B., and Eady, R. R. (2005) *Biochemistry* **44,** 8664–8672
42. Deinum, G., Stone, J. R., Babcock, G. T., and Marletta, M. A. (1996) *Biochemistry* **35,** 1540–1547
43. Fan, B. C., Gupta, G., Danziger, R. S., Friedman, J. L., and Rousseau, D. L. (1998) *Biochemistry* **37,** 1178–1184
44. Franzen, S., Bohn, B., Poyart, C., DePillis, G., Boxer, S. G., and Martin, J. L. (1995) *J. Biol. Chem.* **270,** 1718–1720
45. Franzen, S., Boxer, S. G., Dyer, R. B., and Woodruff, W. H. (2000) *J. Phys. Chem. B.* **104,** 10359–10367
46. Cao, W., Ye, X., Sjodin, T., Christian, J. F., Demidov, A. A., Berezhna, S., Wang, W., Barrick, D., Sage, J. T., and Champion, P. M. (2004) *Biochemistry* **43,** 11109–11117
47. Wyllie, G. R. A., Schulz, C. E., and Scheidt, W. R. (2003) *Inorg. Chem.* **42,** 5722–5734
48. Brucker, E. A., Olson, J. S., Ikeda-Saito, M., and Phillips, G. N. (1998) *Proteins* **30,** 352–356
49. Kitagawa, T. (1988) in *Biological Applications of Raman Spectroscopy* (Spiro, T. G., ed) Vol. 3, pp. 97–131, Wiley Interscience, New York
50. Mitchell, M. L., Li, X. Y., Kincaid, J. R., and Spiro, T. G. (1987) *J. Phys. Chem.* **91,** 4690–4696
51. Li, X. Y., Czernuszewicz, R. S., Kincaid, J. R., Stein, P., and Spiro, T. G. (1990) *J. Phys. Chem.* **94,** 47–61
52. Tsubaki, M., and Yu, N. T. (1982) *Biochemistry* **21,** 1140–1144
53. Duprat, A. F., Traylor, T. G., Wu, G. Z., Coletta, M., Sharma, V. S., Walda, K. N., and Magde, D. (1995) *Biochemistry* **34,** 2634–2644
54. Brunori, M., Cutruzzola, F., Savino, C., Travaglini-Allocatelli, C., Vallone, B., and Gibson, Q. H. (1999) *Biophys. J.* **76,** 1259–1269
55. Shreve, A. P., Franzen, S., Simpson, M. C., and Dyer, R. R. (1999) *J. Phys. Chem. B* **103,** 7969–7975
56. Ionascu, D., Gruia, F., Ye, X., Yu, A. C., Rosca, F., Beck, C., Demidov, A., Olson, J. S., and Champion, P. M. (2005) *J. Am. Chem. Soc.* **127,** 16921–16934
57. Lawson, D. M., Stevenson, C. E. M., Andrew, C. R., and Eady, R. (2000) *EMBO J.* **19,** 5661–5671
58. Marti, M. A., Capece, L., Crespo, A., Doctorovich, F., and Estrin, D. A. (2005) *J. Am. Chem. Soc.* **127,** 7721–7728